current issues in molecular biology

MDPI

Article

Synthesis and *In silico* Study of Some New B*is*-[1,3,4]thiadiazolimines and Bis-thiazolimines as Potential Inhibitors for SARS-CoV-2 Main Protease

Sobhi M. Gomha[1,2]*, Sayed M. Riyadh[2,3], Magda H. Abdellattif [4], Tariq Z. Abolibda[1], Hassan M. Abdel-aziz[5], A. A. Nayl[6], Alaa M. Elgohary[7] and Abdo A. Elfiky[7]*

[1)] Department of Chemistry, Faculty of Science, Islamic University of Madinah, Madinah, 42351, Saudi Arabia. t.z.a@iu.edu.sa, smgomha@iu.edu.sa
[2)] Department of Chemistry, Faculty of Science, Cairo University, Giza, 12613, Egypt. riyadh1993@hotmail.com
[3)] Department of Chemistry, Faculty of Science, Taibah University, Al-Madinah Al-Munawarah, 30002, Saudi Arabia.
[4)] Department of Chemistry, College of Science, PO Box 11099, Taif 21944, Saudi Arabia, m.hasan@tu.edu.sa
[5)] Department of Chemistry, Faculty of Science, Bani Suef University, Bani Suef, Egypt, dr_hassan1971@yahoo.com
[6)] Department of Chemistry, College of Science, Jouf University, Sakaka, Aljouf, P.O. Box 2014, Saudi Arabia. aanayel@ju.edu.sa, aanayl@yahoo.con.
[7)] Department of Biophysics, Faculty of Science, Cairo University, Giza, Egypt. dr_abdo@cu.edu.eg (AAE), aelgohary@cu.edu.eg (AME)
* Correspondence: s.m.gomha@cu.edu.eg, smgomha@iu.edu.sa (SMG), dr_abdo@cu.edu.eg (AAE).

Abstract: A novel series of bis-[1,3,4]thiadiazolimines, and bis-thiazolimines, with alkyl linker, were synthesized through general routes from cyclization of 1,1'-(hexane-1,6-diyl)bis(3-phenylthiourea) and hydrazonoyl halides or α-haloketones, respectively. Docking studies were applied to test the binding affinity of the synthesized products against the M^{pro} of SARS-CoV-2. The best compound, **5h**, has average binding energy (-7.50 ±0.58 kcal/mol) better than that of the positive controls O6K and N3 (-7.36 ±0.34 and -6.36 ±0.31 kcal/mol). Also, the docking poses (H-bonds and hydrophobic contacts) of the tested compounds against the M^{pro} using the PLIP web server were analyzed.

Keywords: Bis-(3-phenylthiourea), hydrazonoyl halides; α-haloketones; molecular docking; SARS-CoV-2 M^{pro}.

1. Introduction

Recently, COVID-19 vaccines have been developed and evaluated to be validated in use [1-4]. Thus, many researchers orchestrated their efforts to formulate and construct novel bioactive bis-heterocycles as antiviral agents and other therapeutic effects. It is being reported in the literature that compounds containing bis-thiadiazoles core have attracted considerable interest in the area of drug discovery due to their potential as an antihypertensive α-blocking [5], antimicrobial [6-8], and anticancer [9] activities. In addition, bis-thiazole pharmacophores were reported to reveal various biological activities such as: anti-inflammatory, analgesic, anti-ulcerogenic [10], antiviral [11], antimicrobial [12], antioxidant [13], and anticancer [14]. Moreover, azoles tethered imines are accentuated to investigate new potential drug candidates with diverse therapeutic efficacy such as antibacterial, antimicrobial, antifungal, anticancer, antioxidant, and antiproliferative

activities [15-18]. So, molecular hybridization of imines and azoles is a beneficial approach to structural alteration as a single species of two or more pharmacophores as potential COVID-19 drug candidates [19].

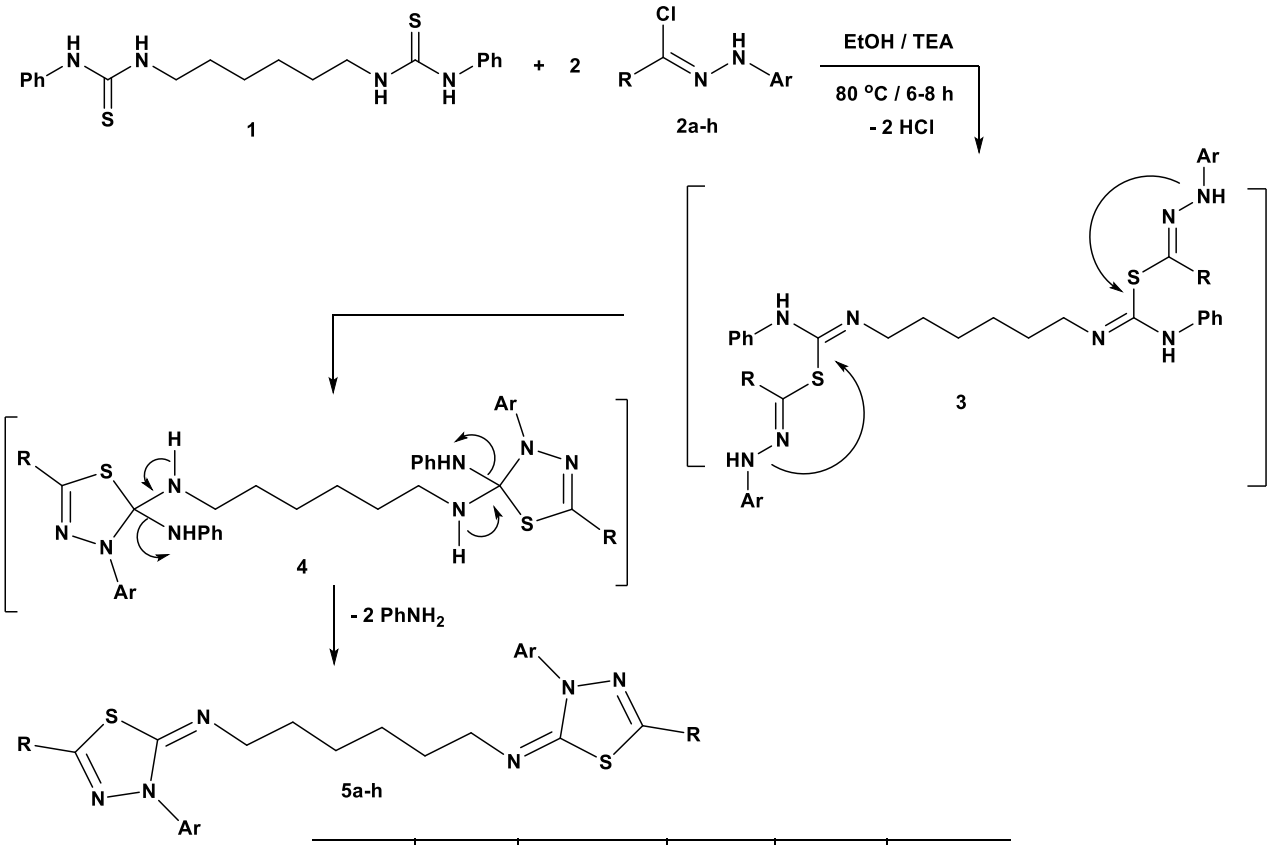
Bis-1,3-thiazole derivatives was examined against different viruses (such as Hepatitis B and C viruses, Poliovirus, and Influenza A virus) and showed promising results (up to EC50 0.56 μM) [20].

The main protease (M^{pro}) or $3CL^{Pro}$ is a vital viral protein that is important for the SARS-CoV-2 life cycle . Its function is to process viral polyprotein upon entry and replication in the host cell [21]. Due to its conservation among different coronaviruses, it is one of the most studied targets in SARS-CoV-2 research, while the dimer form represents the active conformation of the functional enzyme [22-25]. Some drugs are potential candidates that block Mpro function, such as Paxlovid, which was approved for COVID-19 patients in Europe, while others are in clinical trials [26-28].

In this study, the synergism of bis-thiadiazoles or bis-thiazoles with imine moiety in a hybridized molecule has been achieved and docked against the main protease (M^{pro}) of SARS-CoV-2. The docked complexes are examined and analyzed using molecular modeling tools, including molecular docking and dynamics simulation.

2. Results and Discussion

1,1'-(Hexane-1,6-diyl)bis(3-phenylthiourea) (**1**), derived from hexamethylenediamine and phenyl isothiocyanate [29, 30], was allowed to react with hydrazonoyl chlorides **2** in ethanolic solution containing few drops of triethylamine resulting in the formation of *N*,*N*′-(hexane-1,6-diyl)bis[5-substituted-3-aryl-1,3,4-thiadiazol-2(3*H*)-imine] (**5a-h**) as target compounds. The synthetic pathway is depicted in Scheme 1.

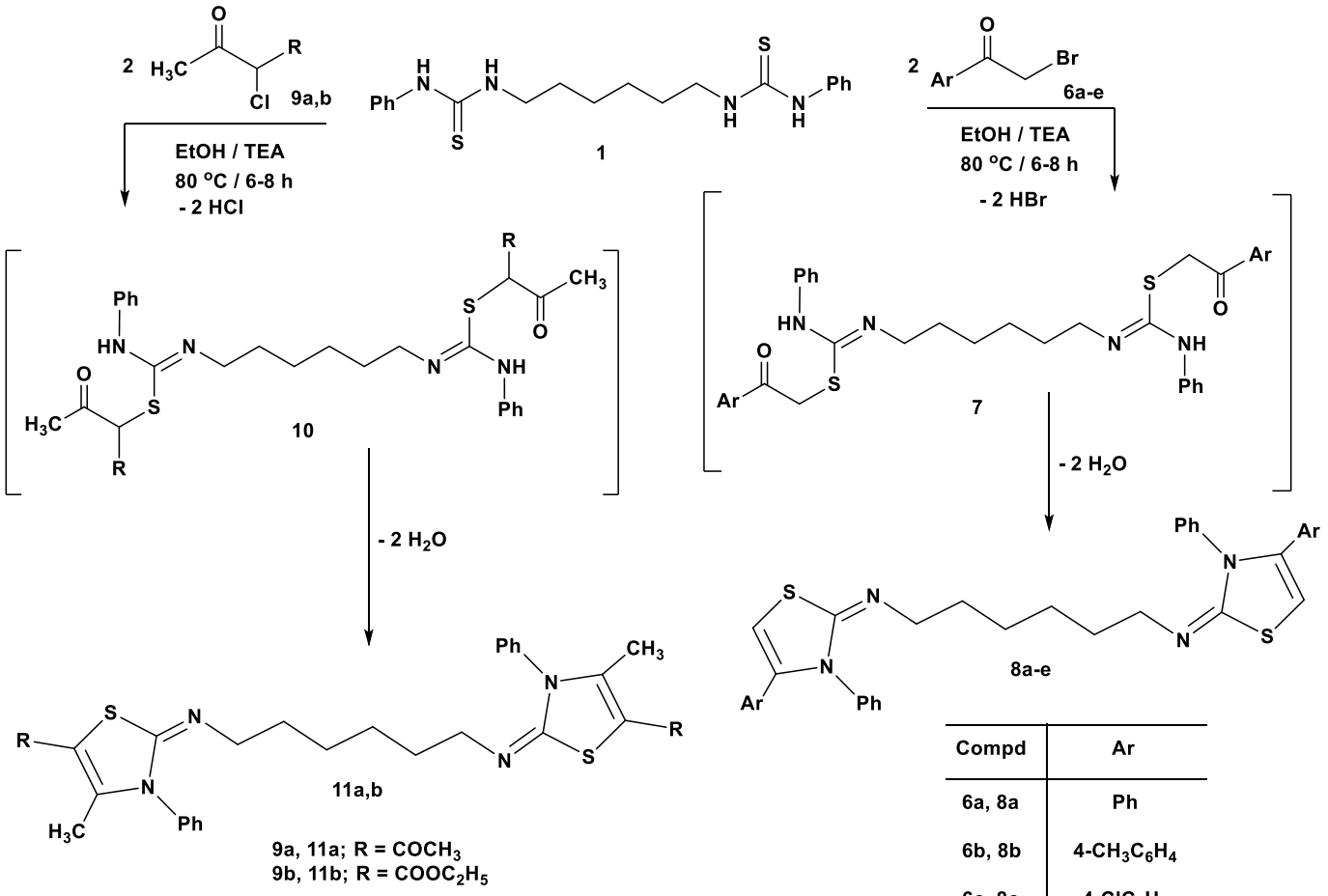


Compd	R	Ar	Compd	R	Ar
2a, 5a	$COCH_3$	Ph	2e, 5e	$COOC_2H_5$	$2\text{-}CH_3C_6H_4$
2b, 5b	$COCH_3$	$4\text{-}CH_3C_6H_4$	2f, 5f	$COOC_2H_5$	$4\text{-}ClC_6H_4$
2c, 5c	$COCH_3$	$4\text{-}ClC_6H_4$	2g, 5g	$COOC_2H_5$	$2,4\text{-}(Cl_2)C_6H_3$
2d, 5d	$COCH_3$	$2,4\text{-}(Cl_2)C_6H_3$	2h, 5h	PhNHCO	Ph

Scheme 1. Synthesis of bis-[1,3,4]thiadiazolimines **5a-h.**

The ~~synthetic strategy~~ of bis-[1,3,4]thiadiazol-2-imines **5a-h** was inaugurated by nucleophilic halogen displacement by the thiol group to afford intermediate **3**. Intramolecular cyclization of the latter intermediate with consecutive elimination of aniline molecules furnished the isolated products in good yields (Scheme 1). The spectroscopic data (IR, ^{1}H-NMR, ^{13}C-NMR, and MS) and the elemental analyses of bis-[1,3,4]thiadiazol-2-imines **5a-h** were in agreement with the assigned structures (see Experimental).

The scope of the previous hetero-cyclization was ~~prolonged~~ with respect to α-haloketones. Thus, we explored the cyclo-condensation reaction of 1,1'-(hexane-1,6-diyl)bis(3-phenylthiourea) (**1**) with substituted phenacyl bromides **6a-e** or 3-chloro-2,4-pentanedione (**9a**) or ethyl 2-chloro-3-oxobutanoate (**9b**) under the employed conditions and the desired bis-thiazol-2-imines **8a-e**, or **11a**, or **11b**, respectively, were obtained in acceptable yields ~~(Scheme 2).~~ This indicated ~~that~~ the synthetic utility of bis(3-phenylthiourea) with an alkyl linker could access bis-heterocyclic scaffolds with expected biological activities. ~~The formation of bis-thiazol-2-imines could be explained by the proposed mechanistic pathway illustrated in Scheme 2.~~



Compd	Ar
6a, 8a	Ph
6b, 8b	4-$CH_3C_6H_4$
6c, 8c	4-ClC_6H_4
6d, 8d	4-BrC_6H_4
6e, 8e	4-$NO_2C_6H_4$

Scheme 2. Synthesis of bis-thiazolimies **8a-e** and **11a.b.**

3. Computational Analysis

Molecular docking combined with molecular dynamics simulation was utilized to test the binding affinity of starting material **1**, bis-[1,3,4]thiadiazol-2-imines **5a-h,** and bis-thiazol-2-imines (**8a-e** and **11a**,b) against the M^{pro} of SARS-CoV-2. The docking was performed after equilibrating the structure for 80 ns MDS run. The reason for performing MDS before docking is that we remove ligands and want the protein to be relaxed before making the docking calculations. We also equilibrate the system and cluster the trajectories to test different possible protein conformations against the compounds. Figure 1A reflects the system equilibration as the root-mean-square deviation (RMSD) curve (blue) is flattened around 2Å. Additionally, the radius of the gyration (RoG) curve (red) is flat during the simulation period, averaging about 26 Å. Figure 1B shows the five representative models for M^{pro} after clustering the trajectories depicted in colored cartoons. Also, the per-residue root-mean-square fluctuations (RMSF) in Å are plotted. The active site residues (H41 and C145) are marked on the RMSF curve. In addition to the protein termini, only one region (S46-M49) shows moderate fluctuations (RMSF > 1.5 Å). This region is red-colored in the structures. The active site residues are away from this region and show low fluctuations (RMSF < 0.7 Å).

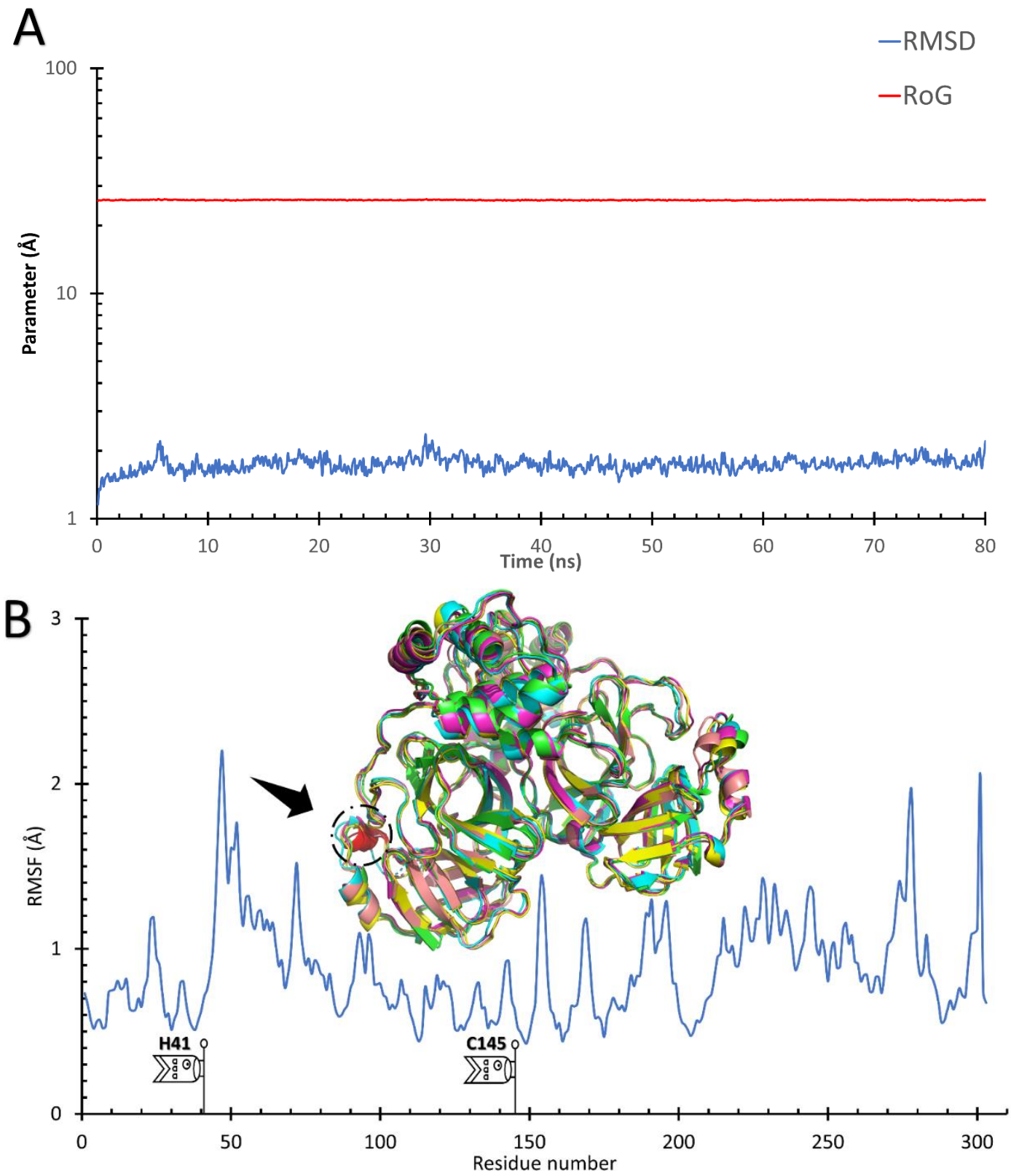
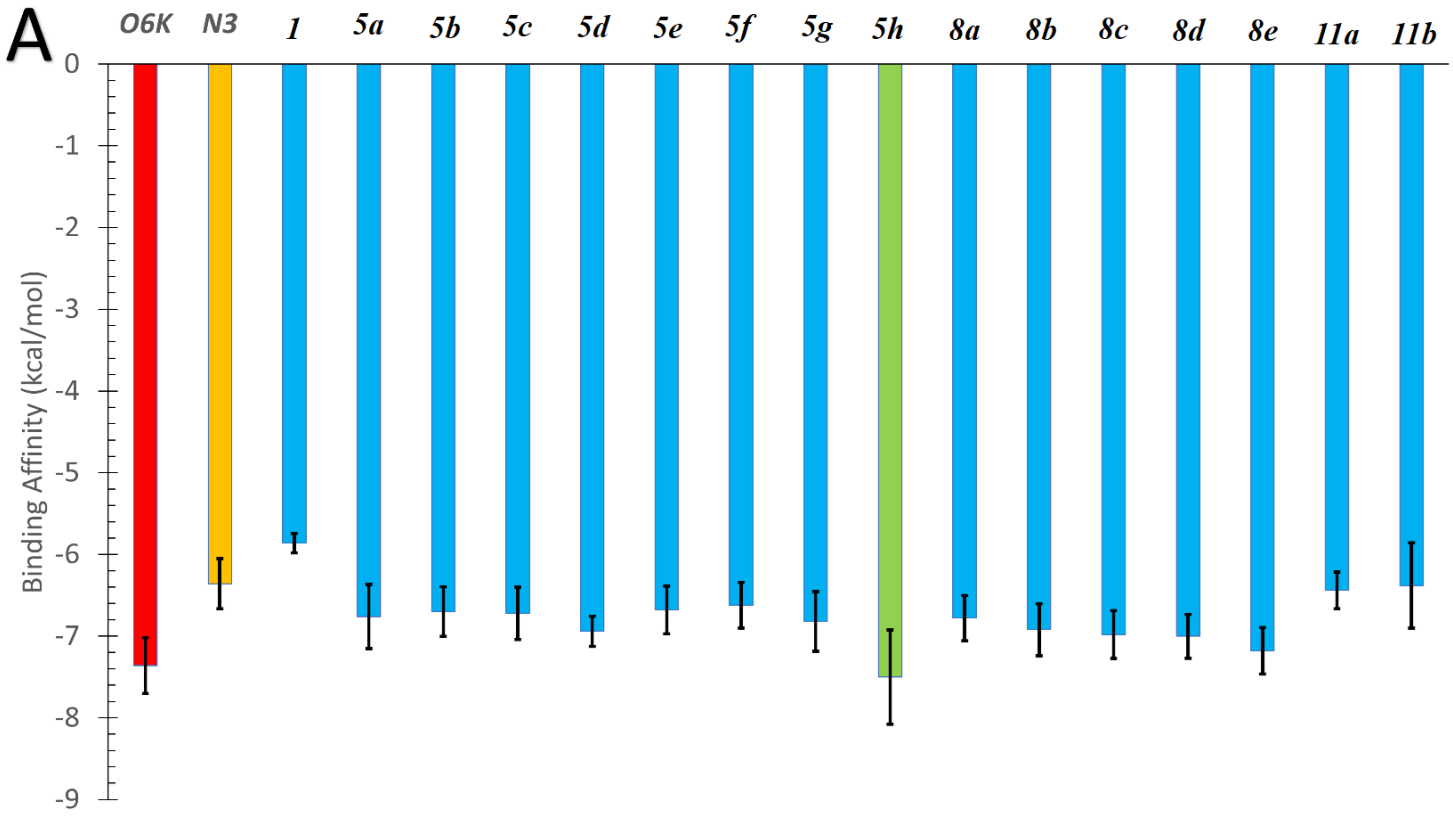
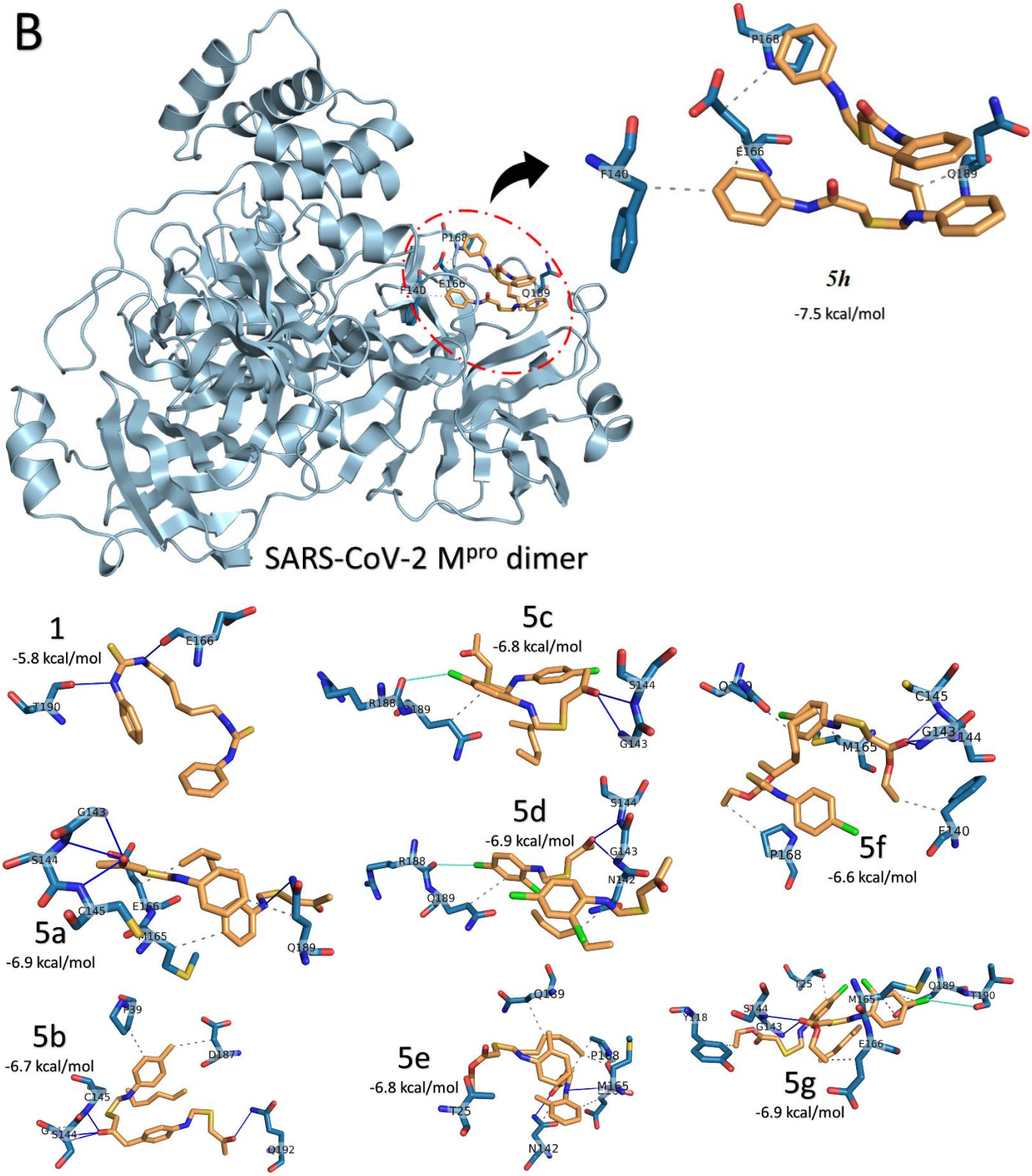


Figure 1. Molecular dynamics simulation analysis. (A) *The root-mean-square deviation (RMSD) (blue) and the radius of gyration (RoG) (red) versus the simulation time.* ***(B)*** *The per-residue root-mean-square fluctuations (RMSF) and the five representative structures of* M^{pro}*. Active site residues (H41 and C145) are marked on the RMSF curve and the structures.*

The bar graph of Figure 2A shows the average (out of five values) binding energy (in kcal/mol) against the Mpro of SARS-CoV-2 different conformations after MDS trajectory clustering. The error bars represent the standard deviation which was calculated by the Microsoft Excel formula $\sqrt{\frac{\Sigma(x-\bar{x})^2}{n-1}}$. Before the docking of the compounds, we tested the docking system by performing a redocking of O6K to the solved structure, and we got a root-mean-square deviation of 0.92 Å (1806 fitted atoms). The positive controls O6K and N3 are shown in red and orange, respectively, while the compounds **1, 5a-h**, **8a-e**, and **11a,b** are in blue (Figure 2A). The best compound, **5h**, is shown in green. The compound **5h** has average binding energy (-7.50 ±0.58 kcal/mol) better than that of the positive controls O6K and N3 (-7.36 ±0.34 and -6.36 ±0.31 kcal/mol). Despite the fact that the binding affinity value of **5h** compound is not significantly different compared to the positive control, it is still a potential anti-SARS-CoV-2 Mpro compound that deserves further investigation.

Figure 2B shows the detailed interaction pattern between **5h** and the Mpro. Five hydrophobic contacts are formed between **5h** and the residues F140, E166(2), P168, and Q189 of Mpro. Additionally, the other compounds (except compound **1**) ~~have more negative (better)~~ binding energies against Mpro (-6.38 ±0.52 down to -7.18 ±0.29 kcal/mol for **11b** and **8e**, respectively) compared to the positive control N3. This reflects their potential to be tightly bound to and might inhibit the Mpro of SARS-CoV-2.




B
SARS-CoV-2 M^{pro} dimer
P168
E166
F140
Q189
5h
-7.5 kcal/mol
1
-5.8 kcal/mol
T190
5c
-6.8 kcal/mol
R188
S144
G143
5d
-6.9 kcal/mol
N142
5f
-6.6 kcal/mol
C145
M165
5a
-6.9 kcal/mol
5b
-6.7 kcal/mol
D187
Q192
5e
-6.8 kcal/mol
T25
5g
-6.9 kcal/mol
Y118

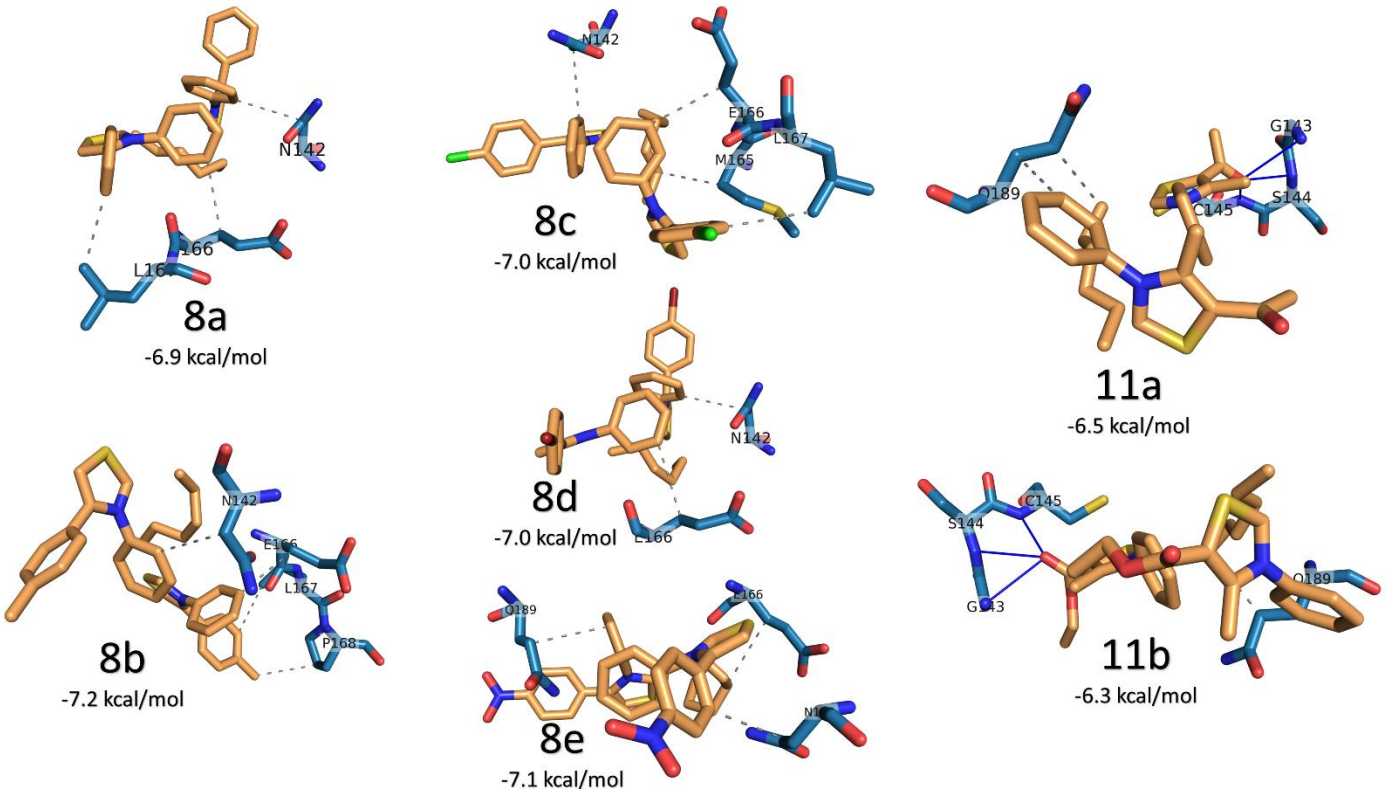


Figure 2. (A) Average binding energies (in kcal/mol) of the positive controls [O6K(red) and N3 (orange)] and compounds **1**, **5a-h**, **8a-e**, and **11a,b** (blue) docked into the active site residues of SARS-CoV-2 M^{pro}. Error bars represent the standard deviations. The best compound in binding the SARS-CoV-2 M^{pro} (**5h**) is shown in green. **(B)** The docking complexes of compounds against SARS-CoV-2 M^{pro} is depicted by PyMOL software.

Further, we analyzed the docking poses of the compounds against the M^{pro} using the PLIP web server, and a detailed list is tabulated (Table 1). ~~We choose~~ ~~the~~ ligand that has the nearest binding affinity to the average value ~~to~~ ~~represent~~ ~~this ligand~~. These modes resemble five different conformations of the protein after an 80 ns MDS run. For the compounds **5a**, **5b**, **5c**, **5d**, **5e**, **5f**, **5g**, **11a**, and **11b,** the most ~~reported~~ interactions are the H-bonds (three) and the hydrophobic contacts (three). On the other hand, only hydrophobic contacts (four) are reported in compounds **5h**, **8a**, **8b**, **8c**, **8d**, and **8e**, while compound **1** formed only two H-bonds with the M^{pro}. Compounds **5c**, **5d**, and **5g** form a halogen bond with R188 or T190 residues of the M^{pro}. The most contributed residues in the formed interactions between the compounds and the Mpro are Q189, E166, N142, G143, S144, and C145, which formed 14, 11, 8, 8, 8, and 5 interactions, respectively.

Table 1. The interaction pattern of the compounds (**1**, **5a-h**, **8a-e**, and **11a,b**) and the positive control O6K against SARS-CoV-2 M^{pro}..

Compd	Binding energy *(kcal/mol)*	***H-bonding* or Halogen bonds**		***Hydrophobic interaction***	
		number	Residues take part in the interaction	number	Residues take part in the interaction
O6K	-7.4	8	S1, **H41**, **G143, S144**, **C145,** H164, and **E166(2)**	4	**N142**, M165, D187, and **Q189**
N3	-6.6	2	H164 and **E166**	3	T25, T26, and P168
1	-5.8	2	**E166** and T190		
5a	-6.9	4	**G143**, **S144**, **C145**, and **Q189**	3	M165, **E166**, and **Q189**
5b	-6.7	4	**G143**, **S144**, **C145**, and Q192	2	P39 and D187

5c	-6.8	2 1	**G143** and **S144** R188	1	**Q189**
5d	-6.9	2 1	**G143** and **S144** R188	2	**N142** and **Q189**
5e	-6.8	2	**N142** and **E166**	6	T25, **N142**, M165, **E166**, P168, and **Q189**
5f	-6.6	3	**G143**, **S144**, and **C145**	4	F140, M165, P168, and **Q189**
5g	-6.9	2 1	**G143** and **S144** T190	5	T25, Y118, M165, **E166**, and **Q189**
5h	**-7.5**			5	F140, **E166(2)**, P168, and **Q189**
8a	-6.9			3	**N142**, **E166**, and L167
8b	-7.2			4	**N142**, **E166**, L167, and P168
8c	-7.0			4	**N142**, M165, **E166**, and L167
8d	-7.0			2	**N142** and **E166**
8e	-7.1			4	**N142**, **E166**, and **Q189(2)**
11a	-6.5	3	**G143**, **S144**, and **C145**	2	**Q189(2)**
11b	-6.3	3	**G143**, **S144**, and **C145**	2	**Q189(2)**

The binding affinities are listed (calculated by AutoDock Vina software) among the number of H-bond, halogen bonds, hydrophobic contacts, and the residues that take part in the interaction. **Bold** residues are the most interacting residue, while the underlined are the active site dyad that forms interactions with the compounds. These residues are important in the protease function as some are the active dyads (underlined), and the others lie within the active site region. When blocked by some small molecules, it may interfere with the protease function (Figure 3), which is yet to be verified in the wet lab.

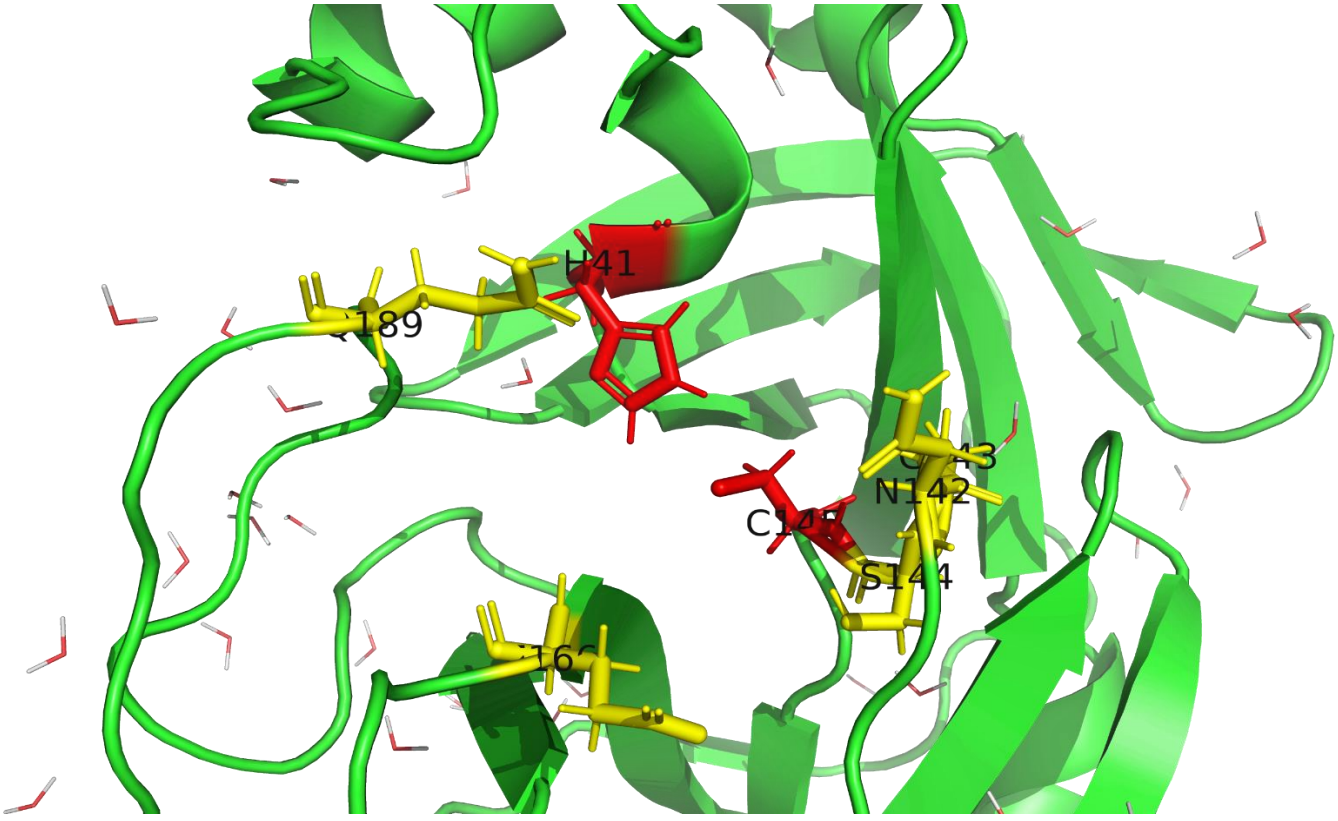
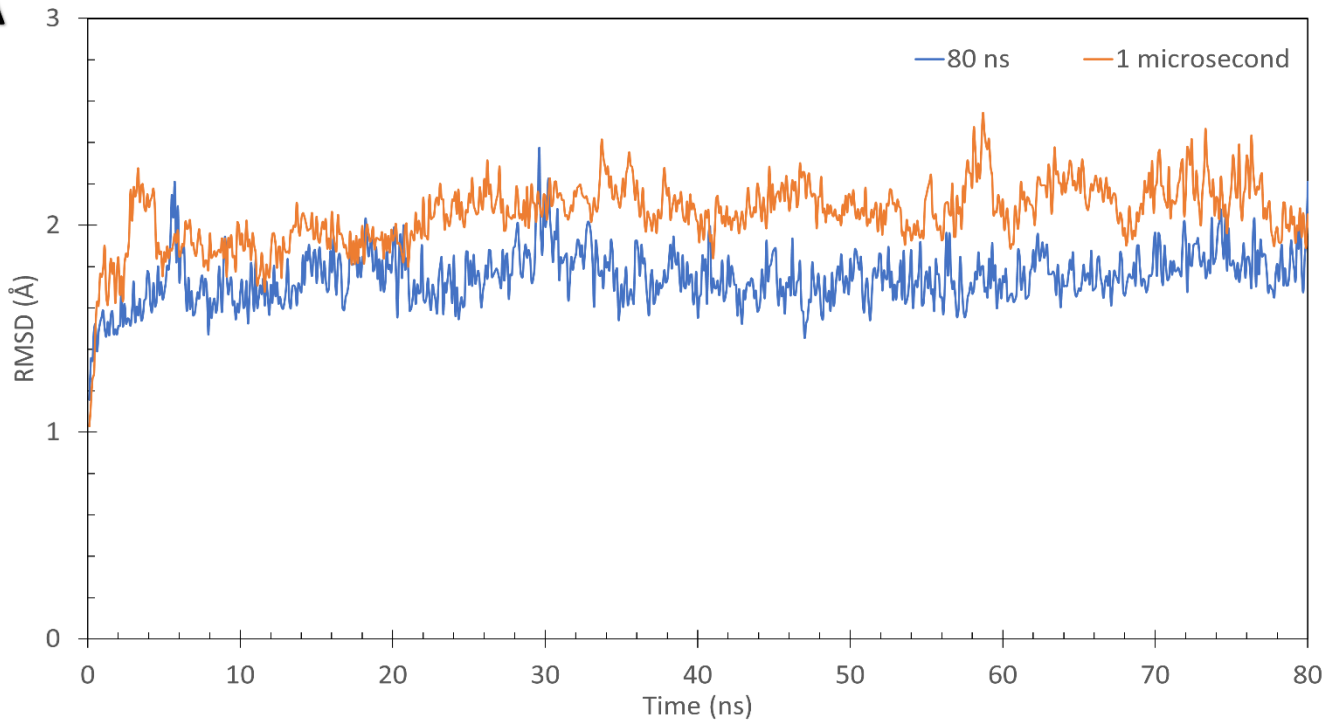


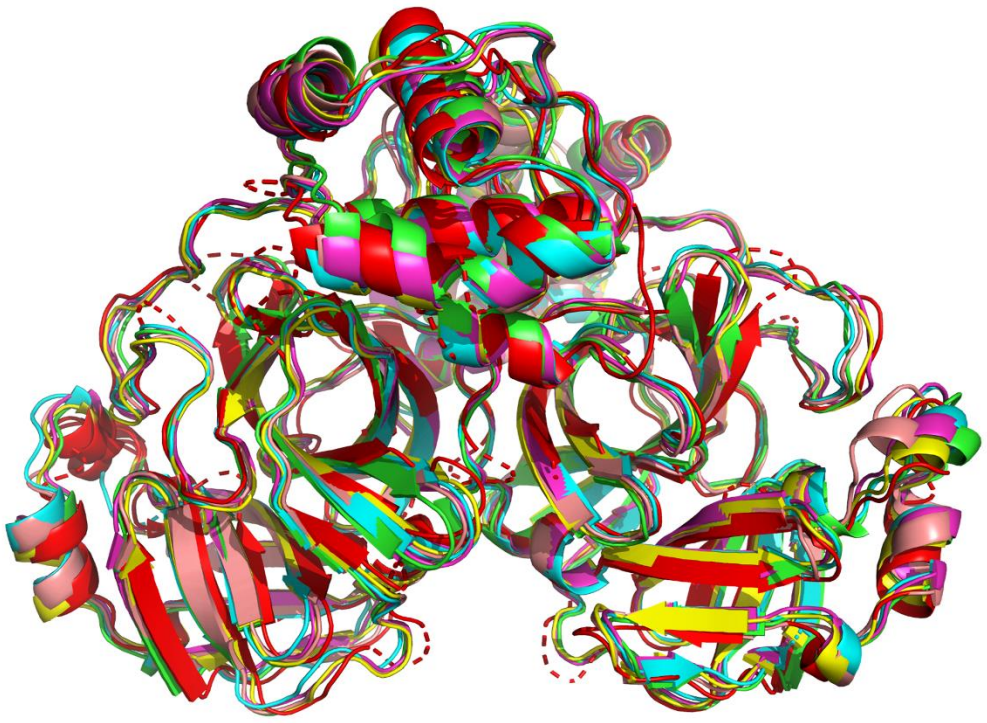
Figure 3 *The most reported interacting residues of SARS-CoV-2 Mpro (green cartoon) with the ligands represented from the solved structure (PDB ID: 6LU7). The active site dyads (H41 and C145) are represented by red sticks, while the yellow sticks represent the most reported interacting residues, N142, G143, S144, E166, and Q189 (underlined in Table 1).*

We trust our simulation as the RMSD of our trajectory coincides with that of the large simulation trajectory found at the following link: (https://figshare.com/search?q=10.6084%2Fm9.figshare.12009789). Figure 4A shows the RMSD of our simulation trajectory (80 ns) in blue and the 1-microsecond trajectory in red. Additionally, we performed blind docking of the compounds utilizing AutoDock Vina implemented in PyRx software against both systems (after trajectory clustering) and found comparable results. The compounds show comparable results to positive controls, and **5h** was the best based on the average binding affinities in both systems.

A



B



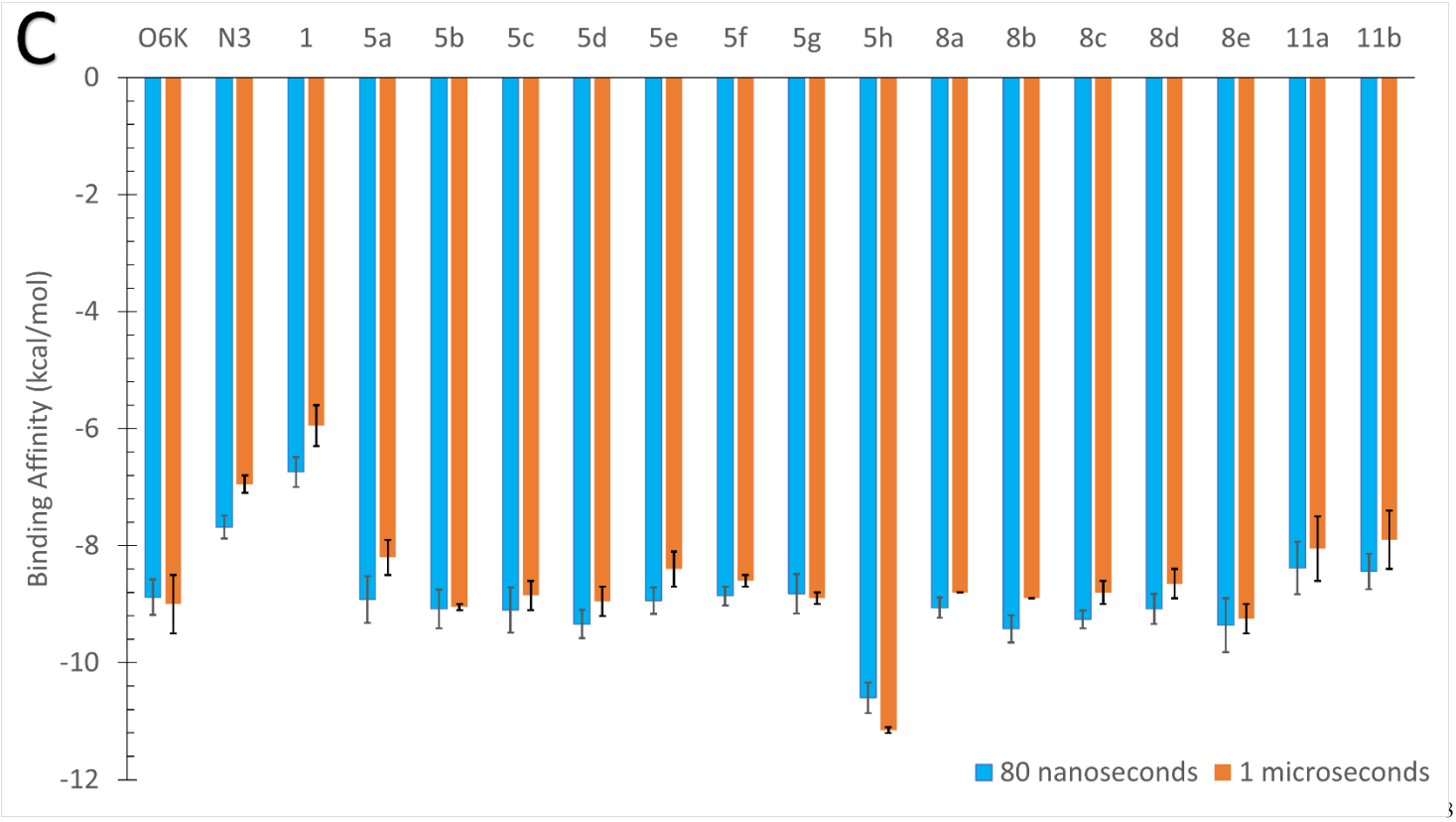


Figure 4 Comparison between the 80 ns and the 1-microsecond trajectories. (A) *the root-mean-square deviation versus the simulation time.* ***(B)*** *the superposition of the most abundant conformation over the 1-microsecond trajectory (red cartoon) with the five different conformations of the 80 ns trajectory (other colored cartoons).* ***(C)*** *The average binding energies that were calculated using AutoDock Vina over PyRx software (blind) for both systems. Error bars represent the standard deviation.*

3.1. Experimental

Melting points were measured on an Electrothermal IA 9000 series digital melting point apparatus. IR spectra were recorded on Pye Unicam SP 3300 and Shimadzu FTIR 8101 PC infrared spectrophotometers. NMR spectra were recorded on a Varian Mercury VX-300 NMR spectrometer operating at 300 MHz (^{1}H NMR) and 75 MHz (^{13}C NMR) and run in deuterated dimethylsulfoxide (DMSO-d_6). Chemical shifts were related to that of the solvent. Mass spectra were recorded on a Shimadzu GCeMS-QP1000 EX mass spectrometer at 70 eV. Elemental analyzes were measured by using a German made Elementar vario LIII CHNS analyzer.

Synthesis of 1,1'-(hexane-1,6-diyl)bis(3-phenylthiourea) (1).

Phenyl isothiocyanate (20 mmol) was added dropwise to a stirred solution of 1,6-diaminohexane (10 mmol) in 30 mL of DMF. The mixture was stirred at room temperature for 3 hours and then added to ice/water mixture. A precipitate was formed was recrystallized from ethanol as colorless crystals.

Yield (96%); m.p. 149-151° (Lit. m.p. 148-149° [29, 30]); IR: υ 3344, 3222 (NH), 1560 (C=N), 1366 (C=S), 976 (C-N) cm^{-1}; ^{1}H-NMR δ = 1.24 (m, 4H, 2CH$_2$), 1.46 (m, 4H, 2CH$_2$), 3.38-3.41 (m, 4H, 2CH$_2$), 7.16-7.42 (m, 10H, Ar-H), 7.62 (br, s, 2H, 2NH), 9.44 (br s, 2H, 2NHPh) ppm; MS m/z (%): 386 (M$^+$, 47). Anal. Calcd. for $C_{20}H_{26}N_4S_2$ (386.16): C, 62.14; H, 6.78; N, 14.49; S, 16.69. Found C, 62.04; H, 6.59; N, 14.33; S, 16.55%.

Synthesis of bis[1,3,4]thiadiazolimines and bis-thiazolimines

A mixture of 1,1'-(hexane-1,6-diyl)bis(3-phenylthiourea) **(1)** (0.386 g, 1 mmol) and appropriate hydrazonoyl halides **2a-h** or α-haloketones **6a-e** or **10a,b** (2 mmol of each) in ethanol (20 mL) containing triethylamine (0.1 g, 1 mmol) was refluxed for 6-8 h. (monitored by TLC). The formed precipitate was isolated by filtration, washed with methanol, dried and recrystallized from EtOH to give products **5a-h** or **8a-e** or **11a,b,** respectively.

1. ,1'-[Hexane-1,6-diyl-bis(azaneylylidene)]bis[(4-phenyl-4,5-dihydro-1,3,4-thiadiazol-2-yl-5-ylidene)]bis(ethan-1-one) (5a).

Yellow crystals (70%); m.p. 173-175 °C; IR: υ 3024, 2932 (C-H), 1691 (C=O), 1623 (C=N) cm^{-1}; ^{1}H-NMR (DMSO-d_6): δ (ppm) 1.04-1.06 (m, 4H, -$CH_2CH_2\underline{CH_2CH_2}CH_2CH_2$-), 1.16-1.21 (m, 4H, -$CH_2\underline{CH_2}CH_2$ $CH_2\underline{CH_2}CH_2$-), 2.44 (s, 6H, $2CH_3$), 3.37-3.42 (m, 4H, -$\underline{CH_2}CH_2CH_2CH_2CH_2\underline{CH_2}$-), 6.97-7.60 (m, 10H, Ar-H); ^{13}C-NMR (DMSO-d_6): δ (ppm) 21.12 (CH_2), 24.36 (CH_3), 26.81 (CH_2), 46.51 (CH_2-N), 124.51, 127.62, 129.21, 133.15, 145.61, 153.11 (Ar-C), 181.42 (C=O); MS *m*/*z* (%): 520 (M^+, 71). Anal. Calcd. for $C_{26}H_{28}N_6O_2S_2$ (520.17): C, 59.98; H, 5.42; N, 16.14; S, 12.31. Found C, 59.80; H, 5.31; N, 16.07; S, 12.19%.

1. ,1'-[Hexane-1,6-diyl-bis(azaneylylidene)]bis[4-(p-tolyl)-4,5-dihydro-1,3,4-thiadiazole-2-yl-5-ylidene)]bis(ethan-1-one) (5b).

Yellow crystals (75%); m.p. 161-163 °C; IR: υ 3025, 2924 (C-H), 1707 (C=O), 1616 (C=N) cm^{-1}; ^{1}H-NMR (DMSO-d_6): δ 1.03-1.05 (m, 4H, -$CH_2CH_2\underline{CH_2CH_2}CH_2CH_2$-), 1.19-1.52 (m, 4H, -$CH_2\underline{CH_2}CH_2$ $CH_2\underline{CH_2}CH_2$-), 2.33 (s, 6H, 2Ar-CH_3), 2.44 (s, 6H, $2CH_3$), 3.37-3.41 (m, 4H, -$\underline{CH_2}CH_2CH_2CH_2CH_2\underline{CH_2}$-), 6.97-7.54 (m, 8H, Ar-H); ^{13}C-NMR (DMSO-d_6): δ (ppm) 21.19 (CH_2), 23.41 (CH_3), 24.28 (CH_3), 26.83 (CH_2), 46.72 (CH_2-N), 124.51, 127.55, 129.74, 132.95, 145.84, 153.17 (Ar-C), 180.81 (C=O); MS *m*/*z* (%): 548 (M^+, 46). Anal. Calcd. for $C_{28}H_{32}N_6O_2S_2$ (548.20): C, 61.29; H, 5.88; N, 15.32; S, 11.69. Found C, 61.16; H, 5.93; N, 15.18; S, 11.75%.

1. ,1'-[Hexane-1,6-diyl-bis(azaneylylidene)]bis[4-(4-chlorophenyl)-4,5-dihydro-1,3,4-thiadiazole-2-yl-5-ylidene)]bis(ethan-1-one) (5c).

Yellow crystals (77%); m.p. 180-182 °C; IR: υ 3022, 2931 (C-H), 1701 (C=O), 1619 (C=N) cm^{-1}; ^{1}H-NMR (DMSO-d_6): δ 1.17-1.21 (m, 4H, -$CH_2CH_2\underline{CH_2CH_2}CH_2CH_2$-), 1.51-1.59 (m, 4H, -$CH_2\underline{CH_2}CH_2$ $CH_2\underline{CH_2}CH_2$-), 2.49 (s, 6H, $2CH_3$), 3.45-3.47 (m, 4H, -$\underline{CH_2}CH_2CH_2CH_2CH_2\underline{CH_2}$-), 6.97-7.64 (m, 8H, Ar-H); ^{13}C-NMR (DMSO-d_6): δ (ppm) 21.18 (CH_2), 24.34 (CH_3), 26.78 (CH_2), 45.81 (CH_2-N), 122.91, 125.62, 129.13, 134.11, 146.61, 153.18 (Ar-C), 183.41 (C=O); MS *m*/*z* (%): 590 (M^++2, 11), 588 (M^+, 38). Anal. Calcd. for $C_{26}H_{26}Cl_2N_6O_2S_2$ (588.09): C, 52.97; H, 4.45; N, 14.26; S, 10.88. Found C, 52.83; H, 4.41; N, 14.11; S, 11.02%.

1,1'-[Hexane-1,6-diyl-bis(azaneylylidene)]bis[4-(2,4-dichlorophenyl)-4,5-dihydro-1,3,4-thiadiazole-2-yl-5-ylidene)]bis(ethan-1-one) (5d).

Yellow crystals (77%); m.p. 179-181 °C; IR: υ 3028, 2921 (C-H), 1704 (C=O), 1617 (C=N) cm^{-1}; ^{1}H-NMR (DMSO-d_6): δ 1.17-1.22 (m, 4H, -$CH_2CH_2\underline{CH_2CH_2}CH_2CH_2$-), 1.51-1.58 (m, 4H, -$CH_2\underline{CH_2}CH_2$ $CH_2\underline{CH_2}CH_2$-), 2.43 (s, 6H, $2CH_3$), 3.41-3.47 (m, 4H, -$\underline{CH_2}CH_2CH_2CH_2CH_2\underline{CH_2}$-), 6.96-7.68 (m, 6H, Ar-H); ^{13}C-NMR (DMSO-d_6): δ (ppm) 21.88 (CH_2), 25.11 (CH_3), 28.80 (CH_2), 45.94 (CH_2-N), 123.51, 125.62, 126.21, 127.15, 131.61, 132.54, 141.41, 154.11 (Ar-C), 184.42 (C=O); MS *m*/*z* (%): 660 (M^++4, 4), 658 (M^++2, 14), 656 (M^+, 35). Anal. Calcd. for $C_{26}H_{24}Cl_4N_6O_2S_2$ (656.02): C, 47.43; H, 3.67; N, 12.76; S, 9.74. Found C, 47.37; H, 3.54; N, 12.66; S, 9.61%.

Diethyl 5,5'-[hexane-1,6-diyl-bis(azaneylylidene)]-bis[4-(o-tolyl)-4,5-dihydro-1,3,4-thiadiazole-2-carboxylate] (5e).

Yellow crystals (72%); m.p. 192-194 °C; IR: *v* 3028, 2927 (C-H), 1728 (C=O), 1612 (C=N) cm^{-1}; ^{1}H-NMR (DMSO-d_6): δ 1.19-1.20 (t, 6H, 2$CH_2\underline{CH_3}$), 1.23-1.35 (m, 4H, -$CH_2CH_2\underline{CH_2CH_2}CH_2CH_2$-), 1.55-1.58 (m, 4H, -$CH_2\underline{CH_2}CH_2CH_2\underline{CH_2}CH_2$-), 2.34 (s, 6H, 2Ar-$CH_3$), 3.45-3.47 (m, 4H, -$\underline{CH_2}CH_2CH_2CH_2CH_2\underline{CH_2}$-), 4.32-4.39 (q, 4H, 2$\underline{CH_2}CH_3$), 6.97-7.42 (m, 8H, Ar-H); ^{13}C-NMR (DMSO-d_6): δ (ppm) 14.84 ($\underline{CH_3}$-CH_2-O), 21.19 (CH_2), 23.11 (Ar-CH_3), 26.77 (CH_2), 46.72 (CH_2-N), 56.17 (CH_3-$\underline{CH_2}$-O), 120.51, 123.55, 126.74, 129.42, 132.11, 133.54, 142.84, 154.17 (Ar-C), 171.81 (C=O); MS *m*/*z* (%): 608 (M^+, 19). Anal. Calcd. for $C_{30}H_{36}N_6O_4S_2$ (608.22): C, 59.19; H, 5.96; N, 13.81; S, 10.53. Found C, 59.13; H, 5.79; N, 13.74; S, 10.68%.

Diethyl 5,5'-[hexane-1,6-diyl-bis(azaneylylidene)]-bis[4-(4-chlorophenyl)-4,5-dihydro-1,3,4-thiadiazole-2-carboxylate] (5f).

Yellowish brown crystals (76%); m.p. 177-179 °C; IR (KBr): *v* 3039, 2927 (CH), 1731 (C=O), 1601 (C=N) cm^{-1}; ^{1}H-NMR (DMSO-d_6): δ 1.18-1.21 (t, 6H, 2$CH_2\underline{CH_3}$), 1.24-1.33 (m, 4H, -$CH_2CH_2\underline{CH_2CH_2}CH_2CH_2$-), 1.55-1.67 (m, 4H, -$CH_2\underline{CH_2}CH_2CH_2\underline{CH_2}CH_2$-), 3.45-3.47 (m, 4H, -$\underline{CH_2}CH_2CH_2CH_2CH_2\underline{CH_2}$-), 4.32-4.39 (q, 4H, 2$\underline{CH_2}CH_3$), 6.99-7.44 (m, 8H, Ar-H); ^{13}C-NMR (DMSO-d_6): δ (ppm) 14.88 ($\underline{CH_3}$-CH_2-O), 21.17 (CH_2), 26.77 (CH_2), 46.76 (CH_2-N), 56.52 (CH_3-$\underline{CH_2}$-O), 121.51, 126.74, 129.11, 135.54, 146.84, 155.17 (Ar-C), 170.11 (C=O); MS *m*/*z* (%): 478 (M^{+}+ 2, 11), 650 (M^++2, 6), 648 (M^+, 14). Anal. Calcd. for $C_{28}H_{30}Cl_2N_6O_4S_2$ (648.11): C, 51.77; H, 4.66; N, 12.94; S, 9.87. Found C, 51.59; H, 4.72; N, 13.02; S, 10.05%.

Diethyl 5,5'-[hexane-1,6-diyl-bis(azaneylylidene)]-bis[4-(2,4-dichlorophenyl)-4,5-dihydro-1,3,4-thiadiazole-2-carboxylate] (5g).

Brown solid (78%); m.p. 192-194 °C; IR (KBr): *v* 3064, 2927 (CH), 1728 (C=O), 1603 (C=N) cm^{-1}; ^{1}H-NMR (DMSO-d_6): δ 1.18-1.23 (t, 6H, 2$CH_2\underline{CH_3}$), 1.28-1.36 (m, 4H, -$CH_2CH_2\underline{CH_2CH_2}CH_2CH_2$-), 1.55-1.64 (m, 4H, -$CH_2\underline{CH_2}CH_2CH_2\underline{CH_2}CH_2$-), 3.43-3.46 (m, 4H, -$\underline{CH_2}CH_2CH_2CH_2CH_2\underline{CH_2}$-), 4.37-4.39 (q, 4H, 2$\underline{CH_2}CH_3$), 6.86-7.81 (m, 6H, Ar-H); ^{13}C-NMR (DMSO-d_6): δ (ppm) 14.11 ($\underline{CH_3}$-CH_2-O), 21.19 (CH_2), 26.68 (CH_2), 46.68 (CH_2-N), 56.64 (CH_3-$\underline{CH_2}$-O), 123.51, 125.74, 126.11, 131.54, 133.58, 141.84, 148.17, 154.17 (Ar-C), 170.13 (C=O); MS *m*/*z* (%): 720 (M^++4, 4), 718 (M^++2, 14), 716 (M^+, 35). Anal. Calcd. for $C_{28}H_{28}Cl_4N_6O_4S_2$ (716.04): C, 46.81; H, 3.93; N, 11.70; S, 8.92. Found C, 46.71; H, 3.80; N, 11.57; S, 8.79%.

5,5'-[Hexane-1,6-diyl-bis(azaneylylidene)]bis[*N*,4-diphenyl-4,5-dihydro-1,3,4-thiadiazole-2-carboxamide] (5h).

Yellow solid (75%); m.p. 188-190 °C; IR (KBr): *v* 3271 (NH), 3025, 2924 (C-H), 1644 (C=O), 1602 (C=N) cm^{-1}; ^{1}H-NMR (DMSO-d_6): δ (ppm) 1.03-1.05 (m, 4H, -$CH_2CH_2\underline{CH_2CH_2}CH_2CH_2$-), 1.19-1.23 (m, 4H, -$CH_2\underline{CH_2}CH_2$ $CH_2\underline{CH_2}CH_2$-), 3.37-3.42 (m, 4H, -$\underline{CH_2}CH_2CH_2CH_2CH_2\underline{CH_2}$-), 6.97-7.54 (m, 20H, Ar-H), 10.42 (s, 2H, 2NH); ^{13}C-NMR (DMSO-d_6): δ (ppm) 21.08 (CH_2), 25.81 (CH_2), 44.51 (CH_2-N), 121.51, 123.62, 126.21, 127.71, 128.15, 131.55, 133.57, 137.64, 146.61, 155.11 (Ar-C), 161.42 (C=O); MS *m*/*z* (%): 674 (M^+, 38). Anal. Calcd. for $C_{36}H_{34}N_8O_2S_2$ (674.22): C, 64.07; H, 5.08; N, 16.60; S, 9.50. Found C, 64.12; H, 5.03; N, 16.42; S, 9.39%.

***N*,*N*'-(Hexane-1,6-diyl)bis[3,4-diphenylthiazol-2(3*H*)-imine] (8a).**

Yellow solid (76%); m.p. 171-173 °C; IR (KBr): *v* 2924 (C-H), 1578 (C=N) cm^{-1}; ^{1}H-NMR (DMSO-d_6): δ 1.02-1.05 (m, 4H, -$CH_2CH_2\underline{CH_2CH_2}CH_2CH_2$-), 1.19-1.23 (m, 4H, -$CH_2\underline{CH_2}CH_2$ $CH_2\underline{CH_2}CH_2$-), 3.43-3.55 (m, 4H, -$\underline{CH_2}CH_2CH_2CH_2CH_2\underline{CH_2}$-), 6.99-7.95 (m, 22H, Ar-H & thiazole-H); ^{13}C-NMR (DMSO-d_6): δ (ppm) 21.11 (CH_2), 24.81 (CH_2), 46.31 (CH_2-N), 122.51, 124.62, 125.21, 127.71, 128.15, 128.94, 129.55, 131.27, 134.57, 137.64, 158.11 (Ar-C); MS *m*/*z* (%): 586 (M^+, 18). Anal. Calcd. for $C_{36}H_{34}N_4S_2$ (586.22): C, 73.69; H, 5.84; N, 9.55; S, 10.93. Found C, 73.58; H, 5.69; N, 9.38; S, 11.06%.

_N,N_'-(Hexane-1,6-diyl)bis[3-phenyl-4-(p-tolyl)thiazol-2(3_H_)-imine] (8b).

Yellow solid (79%); m.p. 169-171 °C; IR (KBr): υ 2934 (C-H), 1599 (C=N) cm^{-1}; ^{1}H-NMR (DMSO-d_6): δ 1.02-1.06 (m, 4H, -$CH_2CH_2\underline{CH_2CH_2}CH_2CH_2$-), 1.19-1.38 (m, 4H, -$CH_2\underline{CH_2}CH_2$ $CH_2\underline{CH_2}CH_2$-), 2.35 (s, 6H, 2Ar-CH_3), 3.34-3.51 (m, 4H, -$\underline{CH_2}CH_2CH_2CH_2CH_2\underline{CH_2}$-), 6.95-7.84 (m, 20H, Ar-H & thiazole-H); ^{13}C-NMR (DMSO-d_6): δ (ppm) 21.19 (CH_2), 23.31 (CH_3), 26.58 (CH_2), 46.11 (CH_2-N), 122.42, 123.58, 124.11, 125.51, 126.34, 127.52, 128.11, 129.74, 130.95, 135.84, 148.17 (Ar-C); MS *m*/*z* (%): 614 (M^+, 22). Anal. Calcd. for $C_{38}H_{38}N_4S_2$ (614.25): C, 74.23; H, 6.23; N, 9.11; S, 10.43. Found C, 74.14; H, 6.19; N, 9.00; S, 10.51%.

_N,N_'-(Hexane-1,6-diyl)bis[4-(4-chlorophenyl)-3-phenylthiazol-2(3_H_)-imine] (8c).

Yellow solid (82%); m.p. 201-203 °C; IR (KBr): υ 2931 (C-H), 1602 (C=N) cm^{-1}; ^{1}H-NMR (DMSO-d_6): δ 1.02-1.05 (m, 4H, -$CH_2CH_2\underline{CH_2CH_2}CH_2CH_2$-), 1.42-1.51 (m, 4H, -$CH_2\underline{CH_2}CH_2$ $CH_2\underline{CH_2}CH_2$-), 3.29-3.32 (m, 4H, -$\underline{CH_2}CH_2CH_2CH_2CH_2\underline{CH_2}$-), 6.88-7.64 (m, 20H, Ar-H & thiazole-H); ^{13}C-NMR (DMSO-d_6): δ (ppm) 21.15 (CH_2), 26.73 (CH_2), 46.08 (CH_2-N), 122.93, 123.45, 124.11, 125.42, 126.51, 127.11, 128.46, 129.13, 133.11, 146.65, 154.18 (Ar-C); MS *m*/*z* (%): 656 (M^+ +2, 8), 654 (M^+, 25). Anal. Calcd. for $C_{36}H_{32}Cl_2N_4S_2$ (654.14): C, 65.94; H, 4.92; N, 8.54; S, 9.78. Found C, 65.83; H, 4.80; N, 8.39; S, 9.64%.

_N,N_'-(Hexane-1,6-diyl)bis[4-(4-bromophenyl)-3-phenylthiazol-2(3_H_)-imine] (8d).

Yellow solid (79%); m.p. 211-213 °C; IR (KBr): υ 2931 (C-H), 1602 (C=N) cm^{-1}; ^{1}H-NMR (DMSO-d_6): δ 1.04-1.07 (m, 4H, -$CH_2CH_2\underline{CH_2CH_2}CH_2CH_2$-), 1.32-1.41 (m, 4H, -$CH_2\underline{CH_2}CH_2$ $CH_2\underline{CH_2}CH_2$-), 3.41-3.67 (m, 4H, -$\underline{CH_2}CH_2CH_2CH_2CH_2\underline{CH_2}$-), 6.85-7.65 (m, 20H, Ar-H & thiazole-H); ^{13}C-NMR (DMSO-d_6): δ (ppm) 21.11 (CH_2), 26.71 (CH_2), 45.88 (CH_2-N), 122.91, 123.35, 124.09, 125.12, 126.38, 127.11, 128.16, 129.13, 132.89, 145.63, 154.12 (Ar-C); MS *m*/*z* (%): 744 (M^+ +2, 10), 742 (M^+, 26). Anal. Calcd. for $C_{36}H_{32}Br_2N_4S_2$ (742.04): C, 58.07; H, 4.33; N, 7.52; S, 8.61. Found C, 58.19; H, 4.24; N, 7.39; S, 8.72%.

_N,N_'-(Hexane-1,6-diyl)bis[4-(4-nitrophenyl)-3-phenylthiazol-2(3_H_)-imine] (8e).

Yellow solid (77%); m.p. 193-195 °C; IR (KBr): υ 2928 (C-H), 1602 (C=N) cm^{-1}; ^{1}H-NMR (DMSO-d_6): δ 1.04-1.08 (m, 4H, -$CH_2CH_2\underline{CH_2CH_2}CH_2CH_2$-), 1.36-1.52 (m, 4H, -$CH_2\underline{CH_2}CH_2$ $CH_2\underline{CH_2}CH_2$-), 3.36-3.42 (m, 4H, -$\underline{CH_2}CH_2CH_2CH_2CH_2\underline{CH_2}$-), 6.88-8.34 (m, 20H, Ar-H & thiazole-H); ^{13}C-NMR (DMSO-d_6): δ (ppm) 21.54 (CH_2), 26.92 (CH_2), 46.18 (CH_2-N), 122.92, 123.39, 125.09, 126.12, 127.38, 128.11, 129.16, 134.13, 145.89, 147.61, 158.12 (Ar-C); MS *m*/*z* (%): 676 (M^+, 38). Anal. Calcd. for $C_{36}H_{32}N_6O_4S_2$ (676.19): C, 63.89; H, 4.77; N, 12.42; S, 9.47. Found C, 63.75; H, 4.58; N, 12.30; S, 9.57%.

1,1'-[Hexane-1,6-diyl-bis(azaneylylidene)]bis[4-methyl-3-phenyl-2,3-dihydrothiazole-5-yl-2-ylidene]bis(ethan-1-one) (11a).

Yellow solid (72%); m.p. 185-187 °C; IR (KBr): υ 2930 (C-H), 1684 (C=O), 1600 (C=N) cm^{-1}; ^{1}H-NMR (DMSO-d_6): δ 1.03-1.05 (m, 4H, -$CH_2CH_2\underline{CH_2CH_2}CH_2CH_2$-), 1.21-1.43 (m, 4H, -$CH_2\underline{CH_2}CH_2$ $CH_2\underline{CH_2}CH_2$-), 2.28 (s, 6H, 2$COCH_3$), 2.55 (s, 6H, 2 thiazole-CH_3), 3.30-3.41 (m, 4H, -$\underline{CH_2}CH_2CH_2CH_2CH_2\underline{CH_2}$-), 6.93-7.35 (m, 10H, Ar-H); ^{13}C-NMR (DMSO-d_6): δ (ppm) 16.85 (thiazole-CH_3), 21.12 (CH_2), 24.33 ($CO\underline{CH_3}$), 26.83 (CH_2), 46.54 (CH_2-N), 118.11, 122.51, 126.62, 129.21, 141.15, 144.61, 154.11 (Ar-C), 181.48 (C=O); MS *m*/*z* (%): 546 (M^+, 20). Anal. Calcd. for $C_{30}H_{34}N_4O_2S_2$ (546.21): C, 65.90; H, 6.27; N, 10.25; S, 11.73. Found C, 65.97; H, 6.09; N, 10.16; S, 11.87%.

Diethyl 2,2'-[hexane-1,6-diyl-bis(azaneylylidene)]-bis[4-methyl-3-phenyl-2,3-dihydrothiazole-5-carboxylate] (11b).

Yellow solid (81%); m.p. 207-209 °C; IR (KBr): υ 2927 (C-H), 1708 (C=O), 1601 (C=N) cm^{-1}; ^{1}H-NMR (DMSO-d_6): δ 1.03-1.05 (m, 4H, -$CH_2CH_2\underline{CH_2CH_2}CH_2CH_2$-), 1.16-1.18 (t,

6H, 2$CH_2\underline{CH_3}$), 1.41-1.48 (m, 4H, -$CH_2\underline{CH_2}CH_2CH_2\underline{CH_2}CH_2$-), 2.57 (s, 6H, 2 thiazole-CH_3), 3.85-3.92 (m, 4H, -$\underline{CH_2}CH_2CH_2CH_2CH_2\underline{CH_2}$-), 4.12-4.16 (q, 4H, 2$\underline{CH_2}CH_3$), 6.89-7.34 (m, 10H, Ar-H); ^{13}C-NMR (DMSO-d_6): δ (ppm) 14.24 ($\underline{CH_3}$-CH_2-O), 17.25 (thiazole-CH_3), 21.18 (CH_2), 26.74 (CH_2), 46.62 (CH_2-N), 56.95 (CH_3-$\underline{CH_2}$-O), 122.51, 126.55, 128.74, 129.40, 143.11, 153.54, 158.17 (Ar-C), 170.11 (C=O); MS *m/z* (%): 606 (M^+, 16). Anal. Calcd. for $C_{32}H_{38}N_4O_4S_2$ (606.23): C, 63.34; H, 6.31; N, 9.23; S, 10.57. Found C, 63.25 H, 6.20; N, 9.18; S, 10.48%.

3.2. Molecular Docking

Compounds are drawn using the Avogadro software 1.2.0, where the universal force field (UFF) was utilized to optimize the structures [31, 32]. The docking was performed using AutoDock Vina software using the flexible ligand in flexible active site (H41 and C145) protocol [33, 34]. SARS-CoV-2 main protease M^{pro} dimer structure (PDB ID: 6Y2G) was downloaded from the protein data bank (https://www.rcsb.org/) [35]. O6K, α-ketoamide inhibitor, is the positive control molecule that was solved in the M^{pro} structure and was used to examine the affinity of the compounds **1**, **5a-h**, **8a-e**, and **11a,b** to the M^{pro} active site. O6K is a covalently bound ligand, but we redock it to the solved structure in a non-bonded fashion, and it gives a root-mean-square difference of 0.966 Å. Additionally, the peptidyl Michael acceptor, N3, found in the solved structure of Mpro (PDB ID: 6LU7), is also used as a positive control for comparison [36]. The M^{pro} dimer was subjected to molecular dynamics simulation (MDS) run for 80 nanoseconds as reported [37] before the docking study. The MDS was conducted on the WEBGRO macromolecular simulation utilizing GROningen MAchine for Chemical Simulations (GROMACS) software and CHARMM27 force field [38, 39]. A minimization for 10000 steps of the conjugate gradient is performed before the MDS run. TIP4P water model was used with a constant number of atoms, volume, and temperature (NVT) ensemble in cubic periodic boundary conditions. Na^+ and Cl^- were added to the system for the salt concentration of 154 mM, while the temperature and pressure were adjusted to be 310 K and 1 atm, respectively, to resemble physiological conditions. Clustering of the trajectories was performed using the UCSF Chimera 1.14 software [40]. A representative structure from each cluster was used in testing the binding affinity using AutoDock Vina software [33,41].

The search box was adjusted to cover the active site dyad (H41 and C145) with dimensions of 30 Å × 30 Å × 30 Å centered at (25.2, 47.3, 38.4) Å. Protein-ligand interaction profiler (PLIP) webserver (https://plip-tool.biotec.tu-dresden.de/plip-web/plip/index) was utilized to check the binding modes, and the data are tabulated and then represented using PyMOL software 2.0.4 in the results section [42-44]. In the current study, we used an exhaustiveness value of 100. This is due to the many rotatable bonds we have in some ligands.

4. Conclusion

The present study disclosed the preparation of 1,1'-(hexane-1,6-diyl)bis(3-phenylthiourea) which was employed as a key intermediate for the synthesis of a new series of bis-[1,3,4]thiadiazolimines, and bis-thiazolimines, with alkyl linker, through its reaction with various hydrazonoyl halides or *a*-haloketones, respectively. The newly synthesized derivatives' structures were confirmed by elemental analysis and spectral data. Docking studies were applied to test the binding affinity of the synthesized products against the M^{pro} of SARS-CoV-2. The study results showed that compound **5h** is the best one, has average binding energy (-7.50 ±0.58 kcal/mol) better than that of the positive controls O6K and N3 (-7.36 ±0.34 and -6.36 ±0.31 kcal/mol). Also, the docking poses (H-bonds and hydrophobic contacts) of the tested compounds against the M^{pro} using the PLIP web server were analyzed. This work paves the way for the design and synthesis

of bis-thiadiazoles, and bis-thiazoles-based libraries, which could lead to the innovation of efficient treatment against SARS-CoV-2 main protease (M^{pro}).

Author Contributions: Sobhi M. Gomha, Sayed M. Riyadh, Magda H. Abdellattif, Tariq Z. Abolibda, Hassan M. Abdel-aziz, A. A. Nayl6, Alaa M. Elgohary and Abdo A. Elfiky: Supervision, Investigation, Methodology, Resources, Formal analysis, Data curation, Funding acquisition, Writing - original draft, Writing - review & editing. All authors have read and agreed to the published version of the manuscript.

Funding: No funding

Institutional Review Board Statement: Not applicable

Informed Consent Statement: Not applicable.

References

1. Gao, Z.; Xu, Y.; Sun, C.; Wang, X.; Guo, Y.; Qiu, S.; Ma, K. A systematic review of asymptomatic infections with COVID-19. *J. Microbiol. Immunol. Infect*. **2021**, *54*, 12–16. DOI: org/10.1016/j.jmii.2020.05.001
2. Yüce, M.; Filiztekin, E.; Özkaya, K.G. COVID-19 diagnosis A review of current methods. *Biosens. Bioelectron*. **2021**, *172*, 112752. DOI: org/10.1016/j.bios.2020.112752
3. Li, Y.; Tenchov, R.; Smoot, J.; Liu, C.; Watkins, S.; Zhou, Q. A Comprehensive Review of the Global Efforts on COVID-19 Vaccine Development. *ACS Cent. Sci*. **2021**, *7*, 512–533. DOI: org/10.1021/acscentsci.1c00120
4. Noor, R. A Review on the Effectivity of the Current COVID-19 Drugs and Vaccines: Are They Really Working Against the Severe Acute Respiratory Syndrome Coronavirus 2 (SARS-CoV-2) Variants? *Curr. Clin. Microbiol. Rep.* **2021**, *8*, 186–193. DOI: org/10.1007/s40588-021-00172-w
5. El-Enany, W. A. M. A.; Gomha, S. M.; El-Ziaty, A. K.; Hussein, W.; Abdulla, M. M.; Hassan, S. A.; Sallam, H. A.; Ali, R. S. Synthesis and molecular docking of some new bis-thiadiazoles as anti-hypertensive α-blocking agents. *Synth. Commun*. **2019**, 1-12. DOI: org/10.1080/00397911.2019.1683207
6. El-Enany, W. A. M. A.; Gomha, S. M.; El-Ziaty, A. K.; Hussein, W.; Sallam, H. A.; Ali, R. S.; El-Ziaty, A. K. Synthesis and Biological Evaluation of Some Novel *Bis*-Thiadiazoles as Antimicrobial and Antitumor Agents. *Polycycl. Aromat. Compds*. **2021**, *41*, 2071-2082. DOI: 10.1080/10406638.2019.1709874
7. Mahmoud, H. K.; Abbas, A. A.; Gomha, S. M. Synthesis, Antimicrobial Evaluation and Molecular Docking of New Functionalized Bis(1,3,4-Thiadiazole) and Bis(Thiazole) Derivatives. *Polycycl. Aromat. Compds*. **2021**, *41*, 2029-2041. DOI: org/10.1080/10406638.2019.1709085
8. Gomha, S. M.; El-Gendy, M. S.; Muhammad, Z. A.; Abdelhamid, A. O.; Abdel-Aziz, M. M. Utility of *Bis*-Hydrazonoyl Chlorides as Precursors for Synthesis of New Functionalized *Bis*-Thiadiazoles as Potent Antimicrobial Agents. *J. Heterocycl. Chem*. **2018**, *55*, 844-851. DOI: org/10.1002/jhet.3108
9. Gomha, S. M.; Kheder, N. A.; Abdelhamid, A. O.; Mabkhot, Y. N. One Pot Single Step Synthesis and Biological Evaluation of Some Novel Bis(1,3,4-thiadiazole) Derivatives as Potential Cytotoxic Agents. *Molecules*, **2016**, *21*: 1532. DOI: 10.3390/molecules21111532
10. Muhammad, Z. A.; Masaret, G.; Amin, M. A.; Abdallah, M. A.; Farghaly, T. A. Anti-inflammatory, Analgesic and Antiulcerogenic Activities of Novel bis-thiadiazoles, bis-thiazoles and bis-formazanes. *Med. Chem*. **2017**, *13*, 226-238. DOI: 10.2174/1573406412666160920091146
11. Dawood, K. M.; Eldebss, T. M. A.; El-Zahabi, H. S. A.; Yousef, M. H. Synthesis and antiviral activity of some new bis-1,3-thiazole derivatives. *Eur. J. Med. Chem*. **2015**, *102*, 266-276. DOI: org/10.1016/j.ejmech.2015.08.005
12. Kassab, R. M.; Gomha, S. M.; Al-Hussain, S. A.; Abo Dena, A. S.; Abdel-Aziz, M. M.; Zaki, M. E. A.; Muhammad, Z. A. Synthesis and In-silico Simulation of Some New Bis-thiazole Derivatives and Their Preliminary Antimicrobial Profile: Investigation of Hydrazonoyl Chloride Addition to Hydroxy-Functionalized Bis-carbazones. *Arabian J. Chem*. **2021**, *14*, 103396. DOI: org/10.1016/j.arabjc.2021.103396
13. Al-Omair, M. A.; Sayed, A. R.; Youssef, M. Synthesis and Biological Evaluation of Bisthiazoles and Polythiazoles. *Molecules*, **2018**, *23*, 1133. DOI: org/10.3390/molecules23051133
14. Dawood, K. M.; Raslan, M. A.; Abbas, A. A.; Mohamed, B. E.; Abdelattif, M. H.; Nafie, M. S.; Hassan, M. K. Novel *Bis*-Thiazole Derivatives: Synthesis and Potential Cytotoxic Activity Through Apoptosis With Molecular Docking Approaches. Front. Chem. 2021, 9, Article 694870. DOI: org/10.3389/fchem.2021.694870
15. Altamimi, M.A.; Hussain, A.; Alshehri, S.; Imam, S.S.; Alnami, A.; Bari, A. Novel hemocompatible imine compounds as alternatives for antimicrobial therapy in pharmaceutical application. *Processes* **2020**, *8*, 1476. DOI: org/10.3390/pr8111476.

16. Bashiri, M.; Jarrahpour, A.; Rastegari, B.; Iraji, A.; Irajie, C.; Amirghofran, Z.; Malek-Hosseini, S.; Motamedifar, M.; Haddadi, M.; Zomorodian, K.; Zareshahrabadi, Z.; Turos, E. Synthesis and evaluation of biological activities of tripodal imines and β-lactams attached to the 1,3,5-triazine nucleus. *Monatsh. Chem*. **2020**, *151*, 821–835. DOI: org/10.1007/s00706-020-02592-8
17. da Silva, E.T.; Araújo, A.S.; Moraes, A.M.; de Souza, L.A.; Lourenço, M.C.S.; de Souza, M.V.N.; Wardell, J.L.; Wardell, S.M.S.V. Synthesis and Biological Activities of Camphor Hydrazone and Imine Derivatives. *Sci. Pharm*. **2016**, *84*, 467. https://doi.org/10.3390/scipharm84030467
18. Sakthinathan, S.P.; Suresh, R.; Kamalakkannan, D.; Mala, V.; Sathiyamoorthi, K.; Vanangamudi, G.; Thirunarayanan, G. Microwave assisted synthesis, spectral correlation and antimicrobial Evaluation of some aryl imines. *J. Chil. Chem. Soc*. **2018**, *63*, 3918–3923. DOI: 10.4067/s0717-97072018000203918
19. Abu-Melha, S.; Edrees, M. M.; Said, M. A.; Riyadh, S. M.; Al-Kaff, N. S.; Gomha, S. M. Potential COVID-19 Drug Candidates Based on Diazinyl-Thiazol-Imine Moieties: Synthesis and Greener Pastures Biological Study. *Molecules* **2022**, *27*, 488. DOI: org/10.3390/molecules27020488
20. Dawood, K. M.; Eldebss, T. M. A .; El-Zahabi, H. S. A.; Yousef, M. H. Synthesis and antiviral activity of some new bis-1,3-thiazole derivatives. *Eur. J. Med. Chem.* **2015**, *102*: 266-276.
21. Zhang, L.; Lin, D.; Sun, X.; Curth, U.; Drosten, C.; Sauerhering, L.; Becker, S.; Rox, K.; Hilgenfeld, R.. Crystal structure of SARS-CoV-2 main protease provides a basis for design of improved α-ketoamide inhibitors. Science 2020, 368, 409-412.
22. Citarella, A.; Scala, A.; Piperno, A.; Micale, N.. SARS-CoV-2 M(pro): A Potential Target for Peptidomimetics and Small-Molecule Inhibitors. Biomolecules , 2021, 11, 607.
23. Goyal, B.; Goyal, D.;. Targeting the Dimerization of the Main Protease of Coronaviruses: A Potential Broad-Spectrum Therapeutic Strategy. ACS Combinatorial Science 2020, 22, 297-305.
24. Jin, Z.; Du, X.; Xu, Y.; Deng, Y.; Liu, M.; Zhao, Y.; Zhang, B.; Li, X.; Zhang, L.; Peng, C.; Duan, Y.; Yu, J.; Wang, L.; Yang, K.; Liu, F.; Jiang, R.; Yang, X.; You, T.; Liu, X.; Yang, X.; Bai, F.; Liu, H.; Liu, X.; Guddat, L.W.; Xu, W.; Xiao, G.; Qin, C.; Shi, Z.; Jiang, H.; Rao, Z.; Yang, H.. Structure of Mpro from SARS-CoV-2 and discovery of its inhibitors. Nature 2020, 582, 289-293.
25. Macip, G.; Garcia-Segura, P.; Mestres-Truyol, J.; Saldivar-Espinoza, B.; Pujadas, G.; Garcia-Vallvé, S.. A Review of the Current Landscape of SARS-CoV-2 Main Protease Inhibitors: Have We Hit the Bullseye Yet? Int. j. of mol. sc. 2021, 23, 259.
26. Abu-Melha, S.; Edrees, M. M.; Riyadh, S. M.; Abdelaziz, M. R.; Elfiky, A. A.; Gomha, S. M. Clean Grinding Technique: A Facile Synthesis and In Silico Antiviral Activity of Hydrazones, Pyrazoles, and Pyrazines Bearing Thiazole Moiety against SARS-CoV-2 Main Protease (Mpro). Molecules 2020, 25, 4565.
27. Burki, T. K. 2022. The role of antiviral treatment in the COVID-19 pandemic. The Lancet Respiratory Medicine 10, e18.
28. Owen, D. R.; Allerton, C. M. N.; Anderson, A. S.; Aschenbrenner, L.; Avery, M.; Berritt, S.; Boras, B.; Cardin, R.D.; Carlo, A.; Coffman, K.J.; Dantonio, A.; Di, L.; Eng, H.; Ferre, R.; Gajiwala, K.S.; Gibson, S.A.; Greasley, S.E.; Hurst, B.L.; Kadar, E.P.; Kalgutkar, A.S.; Lee, J.C.; Lee, J.; Liu, W.; Mason, S.W.; Noell, S.; Novak, J.J.; Obach, R.S.; Ogilvie, K.; Patel, N.C.; Pettersson, M.; Rai, D.K.; Reese, M.R.; Sammons, M.F.; Sathish, J.G.; Singh, R.S.P.; Steppan, C.M.; Stewart, A.E.; Tuttle, J.B.; Updyke, L.; Verhoest, P.R.; Wei, L.; Yang, Q.; Zhu, Y.. An oral SARS-CoV-2 M(pro) inhibitor clinical candidate for the treatment of COVID-19. Science 2021, 374, 1586-1593.
29. Doupp, D.; Hassan, A. A. Thermolysis of *N,N*″-1,ω-alkanediyl-bis[n′-organylthiourea] derivatives. *J. Heterocycl. Chem*. **2006**, *43*, 593-598. DOI: org/10.1002/jhet.5570430311
30. Stoutland, O.; Helgen, L.; Agre, C. L. Reactions of diamines with isocyanates and isothiocyanates. *J. Org. Chem*. **1959**, *24*, 818-820. DOI: org/10.1021/jo01088a022
31. Hanwell, M. D.; Curitis, D. E.; Loniem, D. C.; Vandermeersch, T.; Zurek, E.; Hutchison, G. R. Avogadro: an advanced semantic chemical editor, visualization, and analysis platform. *J. Cheminform*. **2012**, *4*, 17-30. DOI: 10.1186/1758-2946-4-17
32. Rappé, A. K.; Casewit, C. J.; Colwell, K. S.; Goddard, W. A.; Skiff, W. M. UFF, a full periodic table force field for molecular mechanics and molecular dynamics simulations. *J. Am. Chem. Soc*. **1992**, *114*, 10024-10035. DOI: org/10.1021/ja00051a040
33. Trott, O.; Olson, A. J. AutoDock Vina: improving the speed and accuracy of docking with a new scoring function, efficient optimization, and multithreading. *J. Comput. Chem*. **2010**, *31*, 455-461. DOI: 10.1002/jcc.21334
34. Morris, G. M.; Huey, R.; Lindstrom, W.; Sanner, M. F.; Belew, R. K.; Goodsell, D. S.; Olson, A. J. AutoDock4 and AutoDockTools4: Automated docking with selective receptor flexibility. *J. Comput. Chem.* **2009**, *30*, 2785-2791 DOI: org/10.1002/jcc.21256
35. Zhang, L.; Lin, D.; Sun, X.; Curth, U.; Drosten, C.; Sauerhering, L.; Becker, S.; Rox, K.; Hilgenfeld, R. Crystal structure of SARS-CoV-2 main protease provides a basis for design of improved a-ketoamide inhibitors. *Science* **2020**, *368*, 409-412 DOI: 10.1126/science.abb3405
36. Jin, Z.; Jin, Z.; Du, X.; Xu, Y.; Deng, Y.; Liu, M.; Zhao, Y.; Zhang, B.; Li, X.; Zhang, L.; Peng, C.; Duan, Y.; Yu, J.; Wang, L.; Yang, K.; Liu , F.; Jiang, R.; Yang, X.; You, T.; Liu, X.; Yang, X.; Bai, F.; Liu, H.; Liu, X.; Guddat, L. W.; Xu, W.; Xiao, G.; Qin, C.; Shi, Z.; Jiang, H.; Rao, Z.; Yang, H. Structure of Mpro from SARS-CoV-2 and discovery of its inhibitors. *Nature* **2020**, *582*, 289-293. DOI: 10.1038/s41586-020-2223-y
37. Elgohary, A. M.; Elfiky, A. A.; Pereira, F.; Abd El-Aziz, T. M.; Sobeh, M.; Arafa, R. K.; El-Demerdash, A. Investigating the Structure-Activity Relationship of Marine Polycyclic Batzelladine Alkaloids as Promising Inhibitors for SARS-CoV-2 Main Protease (Mpro). *ChemRxiv*. **2022**, DOI: org/10.26434/chemrxiv

38. Bekker, H.; Berendsen, H. J.; Dijkstra, E. J.; Achterop, S.; Vondrumen, R.; Vanderspol, D.; Sijbers, A.; Keegstra, H.; Renardus, M. K. R. GROMACS - A PARALLEL COMPUTER FOR MOLECULAR-DYNAMICS SIMULATIONS. SINGAPORE, *World Scientific Publishing*, **1993**, 252-256. ISBN (Print) 981-02-1245-3.
39. Huang, J.; MacKerell, A. D. CHARMM36 all-atom additive protein force field: validation based on comparison to NMR data. *J. Comput. Chem*. **2013**, *34*, 2135-2145. DOI: 10.1002/jcc.23354
40. Pettersen, E. F.; Goddard, T. D.; Huang, C. C.; Couch, G. S.; Greenblatt, D. M.; Meng, E. C.; Ferrin, T. E. UCSF Chimera—a visualization system for exploratory research and analysis. *J. Comput. Chem*. **2004**, *25*, 1605-1612. DOI: org/10.1002/jcc.20084
41. Elfiky, A. A.; Mahran, H. A.; Ibrahim, I. M.; Ibrahim, M. N.; Elshemey, W. M. Molecular dynamics simulations and MM-GBSA reveal novel guanosine derivatives against SARS-CoV-2 RNA dependent RNA polymerase. *RSC Adv*. **2022**, *12*, 2741-2750. DOI: 10.1039/D1RA07447D
42. Seeliger, D.; de Groot, B. L. Ligand docking and binding site analysis with PyMOL and Autodock/Vina. *J. Comput. Aided Mol. Des*. **2010**, *24*, 417-422. DOI: 10.1007/s10822-010-9352-6
43. Adasme, M. F.; Linnemann, K. L.; Bolz, S. N.; Kaiser, F.; Salentin, S.; Haupt, V. J.; Schroeder, M. PLIP 2021: expanding the scope of the protein-ligand interaction profiler to DNA and RNA. *Nucleic Acids Res*. **2021**, *49*, W530-W534. DOI: org/10.1093/nar/gkab294
44. Salentin, S.; Schreiber, S.; Haupt, V. J.; Adasme, M. F.; Schroeder, M. PLIP: fully automated protein–ligand interaction profiler. *Nucleic Acids Res*. **2015**, *43*, W443-W447. DOI: 10.1093/nar/gkv315